Langmuir

Article

pubs.acs.org/Langmuir

A Chiroptical Switch Based on DNA/Layered Double Hydroxide Ultrathin Films

Wenying Shi, Yankun Jia, Simin Xu, Zhixiong Li, Yi Fu, Min Wei,* and Shuxian Shi*

State Key Laboratory of Chemical Resource Engineering, Beijing University of Chemical Technology, Beijing 100029, P. R. China

Supporting Information

ABSTRACT: A highly oriented film was fabricated by layer-by-layer self-assembly of DNA and MgAl-layered double hydroxide nanosheets, and its application in chiroptical switch was demonstrated via intercalation and deintercalation of an achiral molecule into the DNA cavity. DNA molecules are prone to forming an ordered and dispersive state in the interlayer region of rigid layered double hydroxide (LDH) nanosheets as confirmed by scanning electron microscopy and atomic force microscopy. The induced chiroptical ultrathin film (UTF) is achieved via the intercalation of an achiral chromophore [5,10,15,20-tetrakis(4-*N*-methylpyridyl)-porphine tetra(*p*-toluenesulfonate) (TMPyP)] into the spiral cavity of DNA stabilized in the LDH matrix [denoted as TMPyP-$(DNA/LDH)_{20}$]. Fluorescence and circular dichroism spectroscopy are utilized to testify the intercalation of TMPyP into $(DNA/LDH)_{20}$ UTF that involves two steps: the electrostatic binding of TMPyP onto the surface of $(DNA/LDH)_{20}$ followed by intercalation into base pairs of DNA. In addition, the TMPyP-$(DNA/LDH)_{20}$ UTF exhibits good reversibility and repeatability in induced optical chirality, based on the intercalation and deintercalation of TMPyP by alternate exposure to HCl and NH_3/H_2O vapor, which can be potentially used as a chiroptical switch in data storage.

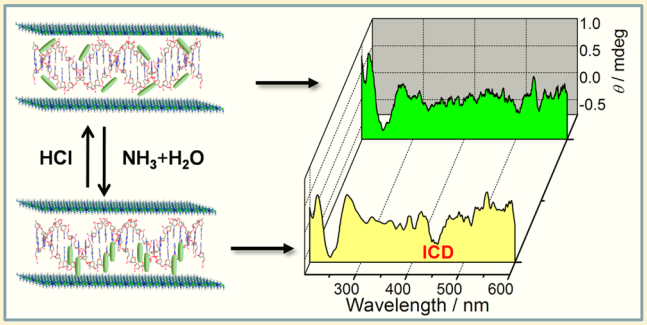

1. INTRODUCTION

Chiroptical switches, which combine optical activity and switchable properties of a system, are promising candidates for application in chiral data storage and memory, chiral molecular recognition, and chiral sensor systems.[1−4] Generally, an intrinsically chiral component (either a chiral trigger, a chiral inducer, or a chiral matrix) is required for the operation of the switch. DNA is one of the most fascinating matrices for inducing chirality of achiral molecules because of the double helix, the intrinsic chirality, and the ability to intercalate various chromophore molecules.[5−7] However, the long chain of DNA generally suffers from coiling as a result of its semirigidity, which greatly limits its application in optical devices. Therefore, a significant challenge in using DNA as a chiral matrix is how to align the individual DNA chain and how to pack a multitude of DNA chains into an ordered structure.[8] Many methods, including hydrodynamic stretching,[9,10] molecular combing,[11] and electrophoretic stretching,[12−15] have been employed to immobilize and orient DNA on a solid matrix. These methods are effective for stretching the individual chain;[16−18] however, they are not feasible for constructing densely packed DNA arrays, which are of interest for the development of optical materials and devices with an enlarged optical signal.

Inorganic nanosheets with a positive or negative charge, which originate from the exfoliation of layered materials, have attracted considerable interest because of their stability, orientation, and restacking property with multifunctional molecules through electrostatic interaction. Among the inorganic nanosheets, the positively charged nanosheets of layered double hydroxides (LDHs) whose structure can be generally expressed as $[M^{II}_{1-x}M^{III}_{x}(OH)_2](A^{n-})_{x/n}\cdot mH_2O$ (M^{II} and M^{III} represent divalent and trivalent metals, respectively, and A^{n-} is an *n*-valent anion)[19,20] have been used successfully as building block to assemble and orient protein molecules because of their low cost and excellent biocompatibility.[21,22] This result shows the ordered arrangement and stability enhancement of protein molecules, which are beneficial for practical application in devices. This inspired us to challenge the goal of aligning individual DNA molecules and constructing a highly oriented and densely packed DNA array via alternate assembly of positively charged LDH nanosheets and negatively charged DNA. The LDH nanosheets provide DNA molecules with a suitable charge match, rigid plane, and stable microenvironment for the dense and ordered stacking, for the purpose of achieving induced chirality of achiral molecules with an enhanced chiral signal via intercalation into the DNA cavity.

In this study, the highly oriented, densely packed DNA was obtained by alternate assembly of DNA and MgAl-LDH nanosheets using the LBL deposition technique (Figure S1 of the Supporting Information). The structural and morphological

Received: March 2, 2014
Revised: September 17, 2014
Published: October 6, 2014

   dx.doi.org/10.1021/la502968z | *Langmuir* 2014, 30, 12916−12922

studies show that the DNA molecules formed an ordered and dispersive state in the interlayer region of rigid LDH nanosheets. The diffraction feature of the UTFs testifies to the formation of a so-called DNA/LDH superlattice structure with long-range stacking order. In addition, an induced chiroptical ultrathin film was achieved via the intercalation of an achiral chromophore [5,10,15,20-tetrakis(4-*N*-methylpyridyl)porphine tetra(*p*-toluenesulfonate) (TMPyP)] into the spiral cavity of DNA stabilized in the LDH matrix. The resulting TMPyP-$(DNA/LDH)_{20}$ UTF exhibits reversible colorimetric behavior and induced circular dichroism (ICD) via alternate exposure of the film in HCl and NH_3/H_2O vapor, which can serve as a chiroptical switch. This solid-state chiroptical switch displays excellent reversibility and photostability. Therefore, this work provides an efficient strategy for the fabrication of DNA with a high level of orientation and dense packing, which can be potentially used as a chiral matrix in nanometer-scale machinery and nonlinear optical devices.

2. EXPERIMENTAL SECTION

2.1. Materials. The sodium salt of double-stranded DNA (dsDNA) from salmon spermary (biochemistry grade) was purchased from Sigma-Aldrich Chemical Co. Analytical grade chemicals, including $Mg(NO_3)_2{\cdot}6H_2O$, $Al(NO_3)_3{\cdot}9H_2O$, formamide, NH_3, H_2O_2, HCl, H_2SO_4, TMPyP, and poly(allylamine hydrochloride) (PAH), were used without further purification. The deionized and decarbonated water was used in all the experimental processes.

2.2. Fabrication of the $(DNA/LDH)_n$ UTFs. The $Mg_2Al\text{-}NO_3$ LDH precursor was synthesized by the hydrothermal method reported previously.[23] A colloidal suspension of exfoliated $Mg_2Al\text{-}NO_3$ LDH nanosheets was obtained by shaking 0.1 g of $Mg_2Al\text{-}NO_3$ LDH in 100 mL of a formamide solution for 24 h. The cleaned quartz glass substrate was obtained by immersion in a concentrated NH_3/30% H_2O_2 mixture (7:3) and concentrated H_2SO_4 for 30 min each. After each procedure, the quartz substrate was rinsed and washed thoroughly with deionized water. The substrate was dipped in a colloidal suspension (0.1 g mL^{-1}) of LDH nanosheets for 10 min and then thoroughly washed, and then the substrate was treated with a 100 mL of a DNA aqueous solution (0.05 wt %) for an additional 10 min followed by washing. Multilayer films of $(DNA/LDH)_n$ were fabricated by alternate deposition of an LDH nanosheet suspension and DNA solution for *n* cycles. The resulting films were dried with a nitrogen gas flow for 2 min at 25 °C.

2.3. Fabrication of the TMPyP-$(DNA/LDH)_n$ UTFs. The $(DNA/LDH)_n$ UTFs were immersed in 2 mM aqueous solutions of TMPyP for various periods of time (from 40 s to 24 h) at different temperature (from 25 to 80 °C). After that, the films were withdrawn from the aqueous solution and rinsed sufficiently with distilled water.

2.4. Characterization Techniques. A Shimadzu T-9201 spectrophotometer is used to record the UV−vis absorption spectra in the range from 200 to 700 nm, with a slit width of 2 nm. The fluorescence emission spectra are collected in range of 550−800 nm, with an excitation wavelength of 500 nm and excitation and emission slits of 5 nm (RF-5301PC). X-ray diffraction (XRD) patterns of the $(DNA/LDH)_n$ UTFs were measured using a Rigaku 2500 VB2+PC diffractometer under the following conditions: 40 kV, 50 mA, Cu Kα radiation (λ = 0.154 nm) step-scanned with a scanning rate of 0.5°/min, and a 2θ angle ranging from 2° to 10°. The morphology of UTFs was investigated by using a scanning electron microscope (SEM ZEISS) and atomic force microscopy (AFM) (Digital Instruments, version 6.12). Circular dichroism (CD) spectra of the UTFs were recorded with a JASCO 720 system. To obtain correct CD spectra, the UTF samples after various treatments were installed perpendicular to the light path and rotated within the film plane to avoid polarization-dependent reflections and eliminate the possible angle dependence of CD signals (Figure S2 of the Supporting Information).[24,25] The component of the UTFs is analyzed by X-ray photoelectron spectroscopy (XPS) with monochromatized A1 Kα exciting X-radiation (PHI Quantera SXM), and Raman spectra with a confocal Raman microspectrometer and excitation at 514.5 nm (Renishaw Instruments Co. Ltd., RM2000).

3. RESULTS AND DISCUSSION

Figure 1A shows the small angle XRD patterns of the as-prepared $(DNA/LDH)_n$ UTFs and exfoliated LDH nanosheets.

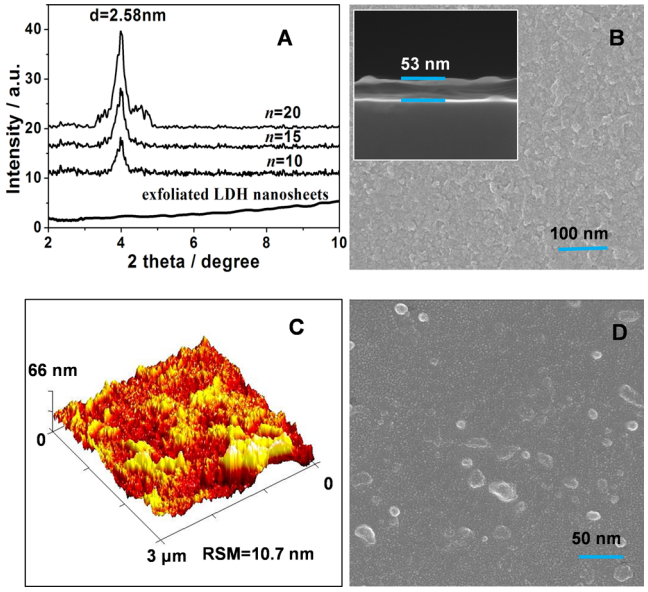

Figure 1. (A) XRD patterns of the exfoliated LDH nanosheets and the $(DNA/LDH)_n$ UTFs (n = 10, 15, and 20). (B) Top view of the SEM image for the $(DNA/LDH)_{20}$ UTF (inset, cross section of the SEM image). (C) AFM image and (D) high-magnification SEM image of the $(DNA/LDH)_{20}$ UTF.

Compared with exfoliated LDH nanosheets, the $(DNA/LDH)_n$ UTFs display a narrow, symmetric, and strong Bragg diffraction reflection at a 2θ value of 3.98°, whose intensity is enhanced linearly along with the increase in bilayer number (Figure S3 of the Supporting Information). According to the theoretical calculation equation of a system with *N* parallel nanosheets, the linear correlation between the basal reflection intensity and bilayer number indicates the formation of superlattice structure.[26] Therefore, the diffraction feature of the $(DNA/LDH)_n$ UTFs can be attributed to a so-called inorganic/organic superlattice structure with long-range stacking order in the normal direction of substrate. The SEM image shows the average repeating distance is ~2.58 nm, which is approximately consistent with the thickness augment per deposited cycle [~2.65 nm (inset of Figure 1B)]. Furthermore, according to thicknesses of ~0.80 nm for a LDH monolayer and 2.01 nm for the diameter of DNA duplex, the DNA/LDH supramolecular structure demonstrates the ideal single-layer arrangement model (Figure S1 of the Supporting Information). The surface morphology of the UTFs was observed by SEM and AFM. The SEM image (Figure 1B) of the $(DNA/LDH)_{20}$ UTF from a top view shows that the film surface is continuous and uniform, with a root-mean-square (rms) roughness of ~10.7 nm obtained by AFM (Figure 1C). A high-magnification SEM image of the $(DNA/LDH)_{20}$ UTF [DNA as the terminal layer (Figure 1D)] demonstrates DNA is well-dispersed. In contrast, an organic polymer PAH was used to assemble the $(DNA/PAH)_{20}$ UTF as a comparison sample (Figure S4 of the

dx.doi.org/10.1021/la502968z | *Langmuir* 2014, 30, 12916−12922

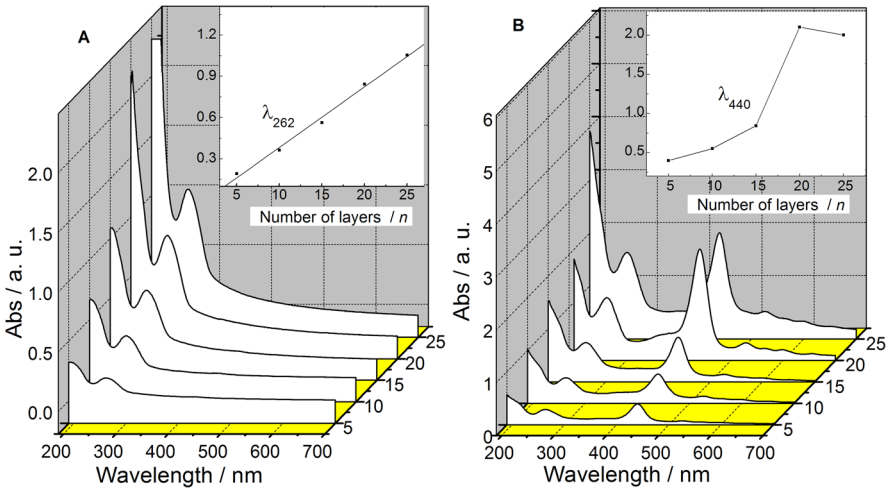

Figure 2. UV−vis absorption spectra of (A) the $(DNA/LDH)_n$ UTFs (n = 5−25) and (B) TMPyP-$(DNA/LDH)_n$ UTFs (n = 5−25). The insets show the absorbance at 262 and 440 nm vs n.

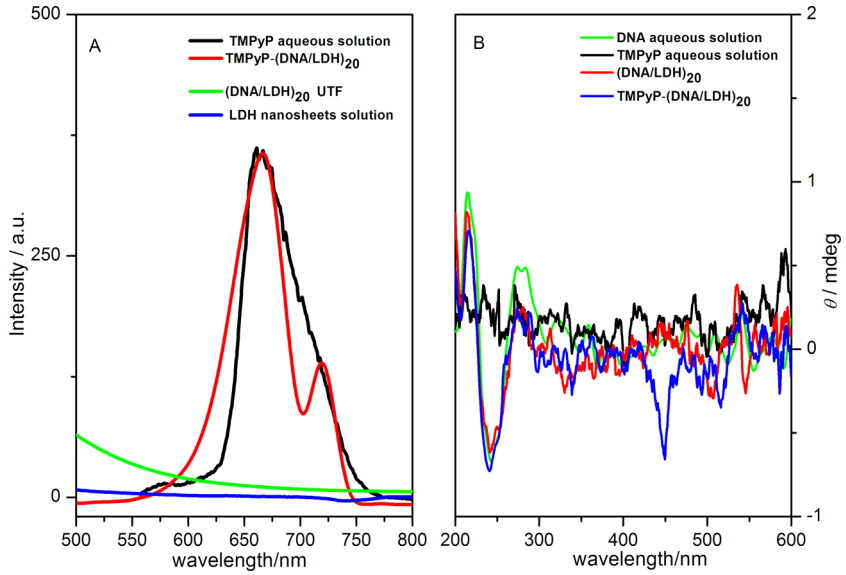

Figure 3. (A) Emission spectra of the TMPyP solution, TMPyP-$(DNA/LDH)_{20}$ UTF, $(DNA/LDH)_{20}$ UTF, and LDH nanosheet sample. (B) CD spectra of the DNA solution, TMPyP solution, $(DNA/LDH)_{20}$ UTF, and TMPyP-$(DNA/LDH)_{20}$ UTF.

Supporting Information), which displays serious aggregation of DNA. The results show the DNA molecules are prone to forming an ordered and dispersive state in the interlayer region of rigid LDH nanosheets.

Figure 2A shows the UV−vis absorption spectra of the $(DNA/LDH)_n$ UTFs with various bilayer numbers (n). It can be found that the absorption bands of DNA at ∼262 nm ($\pi-\pi^*$ transition) correlate linearly with n (inset in Figure 2A), which indicates a stepwise and regular film growth procedure. The absorption spectrum of the $(DNA/LDH)_n$ UTFs is similar to that of the pristine DNA solution sample (Figure S5 of the Supporting Information), excluding the change in the DNA two-dimensional structure during the assembly process. SEM is used to further monitor the deposition process of the $(DNA/LDH)_n$ UTFs (Figure S6A of the Supporting Information). The thicknesses of the as-prepared UTFs (n = 5−20) are in the range of 12−53 nm. Figure S6B of the Supporting Information shows the approximately linear increase in thickness with an increase in the layer number, which confirms the uniform and periodic layered structure of the UTFs present, in agreement with the behavior revealed by the absorption spectra described above. Subsequently, the $(DNA/LDH)_n$ UTFs were immersed in a TMPyP aqueous solution to obtain the TMPyP-$(DNA/LDH)_n$ UTFs. The UV−vis absorption spectra of the TMPyP-$(DNA/LDH)_n$ UTFs display new peaks at 440, 527, 565, and 650 nm attributed to the TMPyP molecule (Figure 2B). This implies the absorption or intercalation of TMPyP in these UTFs.[27,28] To further confirm this issue, we employed the reference sample, $(PSS/LDH)_{20}$ UTF, prepared by the LBL method, to conduct the same test to obtain the TMPyP-$(PSS/LDH)_{20}$ UTF, whose UV−vis absorption and fluorescence emission spectra are shown in Figure S7 of the Supporting Information. The TMPyP-$(PSS/LDH)_{20}$ UTF shows rather weak absorption intensity at 440 nm and no fluorescence emission peak of TMPyP, in comparison with the TMPyP-$(DNA/LDH)_{20}$ UTF, indicating only surface adsorption of TMPyP occurs in the former system while TMPyP undergoes both surface adsorption and intercalation into DNA in the latter. This will be further verified by CD spectra in the next section. The absorption band of the solid TMPyP crystal shows

dx.doi.org/10.1021/la502968z | Langmuir 2014, 30, 12916−12922

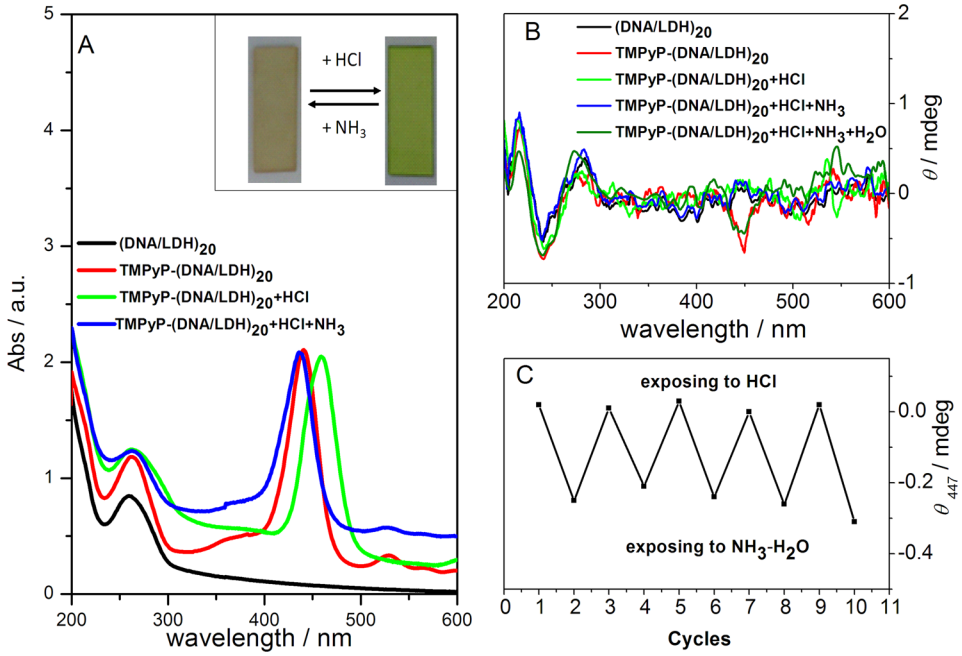

Figure 4. (A) Absorption spectra (inset, photographs), (B) CD spectra, and (C) reversibility of the TMPyP-$(DNA/LDH)_{20}$ UTF recorded after alternate exposure to HCl and NH_3/H_2O vapor.

a red shift of ~33 nm compared with that of its aqueous solution, whereas the absorption band of the intercalated TMPyP is located between the solution and crystal (Figure S5 of the Supporting Information). Moreover, the maximal absorption band of the intercalated TMPyP undergoes a red shift (from 429 to 440 nm) with an increase in immersion time (from 40 s to 24 h) at room temperature (inset in Figure S8A of the Supporting Information). These results indicate that the dense packing of TMPyP molecules in DNA/LDH UTFs leads to some aggregation and the resulting red shift of the absorption band. The nonlinear increase in the intensity of the absorption band of TMPyP at 440 nm along with the thickness of $(DNA/LDH)_n$ UTF shows that the optimal bilayer number is 20 (Figure 2B, inset). Moreover, the change in absorption intensity was also studied by tuning the treatment time and temperature for the intercalation of TMPyP. The absorption intensity at 440 nm displays a slow enhancement with an increase in immersion time (from 40 s to 24 h) of the UTF in the TMPyP solution at room temperature (Figure S8A of the Supporting Information). In contrast, the absorption intensity increases drastically with an increase in temperature from 25 to 70 °C (Figure S8B of the Supporting Information), indicating temperature has a significant influence on the intercalation of TMPyP molecules into the $(DNA/LDH)_n$ UTFs. Therefore, a temperature of 70 °C was chosen in the following section except as specifically illustrated.

To clarify the exact position of TMPyP molecule in the $(DNA/LDH)_{20}$ UTF, the fluorescence emission spectra are measured and shown in Figure 3. Both the LDH nanosheet sample and the $(DNA/LDH)_{20}$ UTF show no emission peak. The TMPyP aqueous solution displays a strong emission at 667 nm, while the TMPyP-$(DNA/LDH)_{20}$ UTF shows a new peak at 718 nm besides that at 669 nm (Figure 3A). The vibrational peak of TMPyP in aqueous solution is not obvious, which is possibly due to the vibronic coupling between the excited singlet state (S_1) and a nearby charge-transfer (CT) state.[29] For the TMPyP-$(DNA/LDH)_{20}$ UTF, however, the emission spectrum includes a vibronic resolution of TMPyP. This can be attributed to the less polar microenvironment provided by the DNA spiral cavity, which hinders the existence of the CT state and the resulting electronic coupling between the S_1 and CT states of TMPyP. Therefore, the variation in TMPyP emission indicates the change in its microenvironment. A previous study of the intercalation of TMPyP into the DNA/poly(allylamine hydrochloride) (DNA/PAH) film reported emission occurs at 669 and 720 nm, indicating TMPyP is intercalated in the G-C site of DNA.[30] For the TMPyP-$(DNA/LDH)_{20}$ UTF studied in this work, it is proposed that TMPyP molecules are not adsorbed on the film surface but intercalate into the spiral cavity of DNA. This is further confirmed by CD spectra (Figure 3B). The positive and negative Cotton effect of the $(DNA/LDH)_{20}$ UTF at 215 and 242 nm is assigned to DNA, which is similar to that of a pristine DNA solution. This indicates that the rigid and confined two-dimensional microenvironment provided by LDH nanosheets facilitates a strong dispersion of DNA molecules. The CD spectrum of the TMPyP aqueous solution shows no peak, demonstrating the absence of a Cotton effect. However, the CD spectrum of the TMPyP-$(DNA/LDH)_{20}$ UTF exhibits a negatively induced Cotton effect at 449 nm, indicating that the TMPyP molecule is intercalated into the spiral cavity of DNA in a manner other than groove binding, because the latter geometry will show a strong and positive ICD peak due to transitions polarized in the direction of the groove.[31−33] Generally, a pair of CD peaks were found for the intercalation of TMPyP into DNA in solution.[34,35] However, only a single peak was observed for the TMPyP-$(DNA/LDH)_{20}$ UTF in this work, implying the microenvironment has influence on the stacking of TMPyP and the resulting CD spectrum. Furthermore, the CD spectrum of the TMPyP-$(DNA/LDH)_{20}$ UTF at room temperature shows no negatively induced Cotton effect at 449 nm (Figure S9 of the Supporting Information), although an absorption at 440 nm attributed to TMPyP is observed. This indicates that TMPyP is only electrostatically adsorbed on the surface of the

dx.doi.org/10.1021/la502968z | Langmuir 2014, 30, 12916−12922

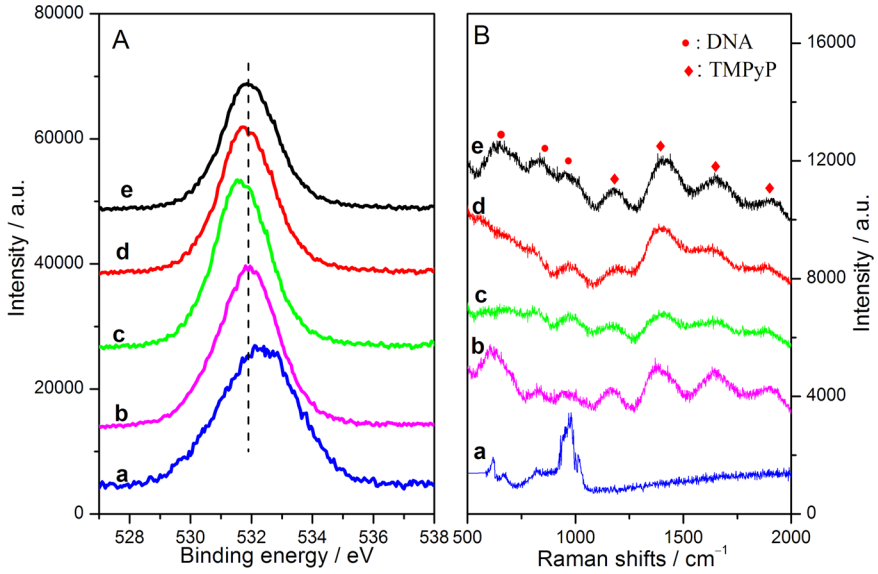

Figure 5. (A) XPS and (B) Raman spectra of (a) the $(DNA/LDH)_{20}$ UTF, (b) the TMPyP-$(DNA/LDH)_{20}$ UTF, (c) the sample of part b exposed to HCl vapor, (d) the sample of part c exposed to NH_3 vapor, and (e) the sample of part d exposed to H_2O vapor.

$(DNA/LDH)_{20}$ UTF at room temperature as it enters into the spiral cavity of DNA at 70 °C. Therefore, the intercalation of TMPyP into the $(DNA/LDH)_{20}$ UTF may involve two steps: the electrostatic binding of the TMPyP to the surface followed by intercalation into base pairs of DNA.

Because the interaction between TMPyP and DNA plays a key role in determining the ordered stacking of TMPyP and induced chirality, the variation in the charge state of TMPyP may cause a change in its packing mode and the resulting chirality signal. In an effort to study the chiral switching performance, the TMPyP-$(DNA/LDH)_{20}$ UTF was treated with HCl and NH_3 vapor to trigger protonated and deprotonated states, respectively. The UV−vis and CD spectra of the TMPyP-$(DNA/LDH)_{20}$ UTF under various vapor conditions were recorded. The TMPyP-$(DNA/LDH)_{20}$ UTF exposed to HCl vapor shows a red shift of the maximal absorption band [from 441 to 458 nm (Figure 4A)] as well as a change in color [from orange to green (inset of Figure 4A)], while the UTF recovers its original absorption wavelength and color after being exposed to NH_3 vapor. After alternate exposure to HCl and NH_3 vapor, both TMPyP and DNA molecules are protonated and deprotonated, respectively. Therefore, the reversible shift in the absorption band of TMPyP can be attributed to the change in microenvironment and aggregation state of TMPyP molecules. In addition, denaturization and reorganization of DNA molecules during the vapor-exposing process can be excluded, because the DNA characteristic absorption at 265 nm shows no shift or change. Figure 4B displays the CD spectra of the TMPyP-$(DNA/LDH)_{20}$ UTF in this process. Upon exposure to HCl vapor, the negatively induced Cotton effect of the TMPyP-$(DNA/LDH)_{20}$ UTF at 449 nm disappeared completely, which is similar to the results of previous studies of the deintercalation of TMPyP from a DNA/PAH film.[28,36] This result indicates that a weak electrostatic interaction between TMPyP and DNA occurs after the deintercalation of TMPyP from the DNA spiral cavity, rather than the groove bond. However, the ICD does not recover upon being exposed to NH_3 vapor, although deprotonation of TMPyP would occur. It is interesting to find that the ICD at 449 nm can be recovered by subsequent exposure of the UTF to H_2O vapor, demonstrating H_2O molecules facilitate the reintercalation of TMPyP into the spiral cavity of DNA. In addition, it can be found that a good repeatability of the UTF was obtained with RSD values of 1.14% (HCl) and 3.64% (NH_3/H_2O) in 10 cycles by alternate exposure to HCl and NH_3/H_2O vapor, respectively (Figure 4C).

The reversible process was further investigated by using XPS and Raman spectra (Figure 5). Compared with the $(DNA/LDH)_{20}$ UTF [C═O, 532.1 eV (Figure 5A-a)], the XPS peak of O 1s for the TMPyP-$(DNA/LDH)_{20}$ UTF [C═O, 531.8 eV (Figure 5A-b)] shifts to a lower binding energy, which can be attributed to the increase in electron density due to the interaction between TMPyP and DNA. The further decreased binding energy of O 1s for the TMPyP-$(DNA/LDH)_{20}$ UTF exposed to HCl gas [C═O, 531.6 eV (Figure 5A-c)] indicates that H^+ imposes an effect on the increase in electron density. After exposure to NH_3, the peak of O 1s shifts to a higher binding energy [C═O, 531.7 eV (Figure 5A-d)]. The XPS of O 1s can be recovered [C═O, 531.8 eV (Figure 5A-e)] by subsequently exposing the UTF to H_2O vapor. The reversible process can be further verified by the results of Raman spectra (Figure 5B). Compared with the $(DNA/LDH)_{20}$ UTF (Figure 5B-a), the TMPyP-$(DNA/LDH)_{20}$ UTF displays new peaks [C−H, 1164 cm^{-1}; C−C, 1403, 1637, and 1905 cm^{-1} (Figure 5B-b)] assigned to the TMPyP molecule,[37,38] which indicates TMPyP was intercalated into the $(DNA/LDH)_{20}$ UTF.[39,40] The peak position of the phosphodiester (O−P−O, 828−830 cm^{-1}) confirms DNA in the TMPyP-$(DNA/LDH)_{20}$ UTF belongs to the B-form with GC-rich sequences.[41] The absence of any variation in this peak during the cycle indicates that the DNA configuration remains unchanged. Moreover, the band at 900−1000 cm^{-1} shows no change, which can be attributed to the retention of backbone and secondary structure of DNA during the cycle.[42] In contrast, the peak in the range of 610−650 cm^{-1} disappeared for the TMPyP-$(DNA/LDH)_{20}$ UTF upon exposure to HCl vapor, demonstrating the disappearance of interaction between dC (and dG) and TMPyP.[43] After exposure to NH_3, no recovery can be observed (Figure 5, curve d). However, a subsequent treatment with H_2O vapor results in

dx.doi.org/10.1021/la502968z | *Langmuir* 2014, 30, 12916−12922

the complete recovery of the Raman spectrum over the whole wavelength range (Figure 5, curve e), indicating H_2O molecules contribute to the intercalation of TMPyP into the spiral cavity of DNA. The results of XPS and Raman spectra further validate the conclusion based on CD and UV spectra. The reversible process is illustrated in Scheme 1.

Scheme 1. Representation of the Intercalation and Deintercalation of TMPyP Molecules in the $(DNA/LDH)_{20}$ UTF (Mg, dark blue; Al, green; H, white; O, blue; C, gray)[a]

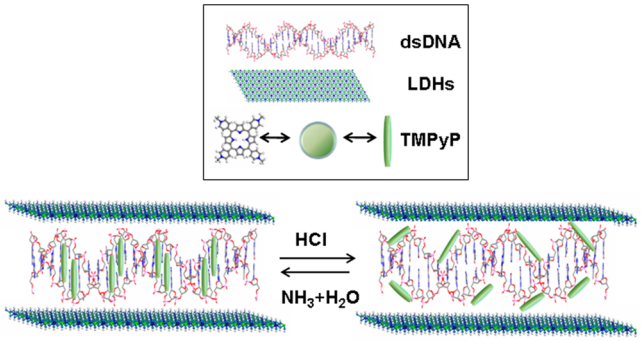

[a]Exposure of the TMPyP-$(DNA/LDH)_{20}$ UTF to HCl vapor results in the protonation and deintercalation of TMPyP; the following treatment with NH_3 and water vapor leads to the reintercalation of TMPyP into the $(DNA/LDH)_{20}$ UTF.

The stability of the UTF is vitally important, which will lead to unreliable and destructive readout and even the breakdown of switch ability in the extreme case. The absorption intensities of the TMPyP-$(DNA/LDH)_{20}$ UTF and pristine TMPyP in solution were collected by illumination under UV light for a comparison study (Figure S10 of the Supporting Information). A remarkable decrease in the absorption intensity of the TMPyP solution was observed after UV irradiation for 1 h, while the TMPyP-$(DNA/LDH)_{20}$ UTF maintained ~95% of its initial absorption intensity. Figure S11 of the Supporting Information shows ~94.3% of its original absorption intensity remained after measurement for 1 month, indicating the high storage stability of the TMPyP-$(DNA/LDH)_{20}$ UTF. The results indicate that a significant enhancement of the photostability and storage stability of the TMPyP molecule in the $(DNA/LDH)_{20}$ UTF matrix has been obtained, which would guarantee its practical application in optical switches.

4. CONCLUSIONS

In summary, $(DNA/LDH)_n$ UTFs with a high orientation and dense packing on quartz substrates were obtained via alternate assembly of DNA and MgAl-LDH nanosheets using the LBL deposition technique. TMPyP molecules enter into the spiral cavity of DNA through electrostatic interaction between DNA and TMPyP, which endows the compound with a new negatively induced Cotton effect at 449 nm attributed to the TMPyP molecule. In addition, the reversible chiroptical performance was achieved on the basis of the intercalation and deintercalation of TMPyP by alternate exposure of the TMPyP-$(DNA/LDH)_{20}$ UTF to HCl and NH_3/H_2O vapor. This chiroptical switch exhibits high stability and chemical reversibility. This strategy can be further extensed, which will allow access to applications in chiral optical switches through fine-tuning compositions for both inorganic LDH and organic chromophores as well as their interactions.

■ ASSOCIATED CONTENT

Supporting Information

Representation of the assembly and structure, SEM image, absorption spectra, CD spectra, and stability data. This material is available free of charge via the Internet at http://pubs.acs.org.

■ AUTHOR INFORMATION

Corresponding Authors

*Phone: +86-10-64412131. Fax: +86-10-64425385. E-mail: weimin@mail.buct.edu.cn.
*E-mail: shisx@mail.buct.edu.cn.

Notes

The authors declare no competing financial interest.

■ ACKNOWLEDGMENTS

This work was supported by the 973 Program (Grant 2014CB932104), the National Natural Science Foundation of China (NSFC), the Scientific Fund from Beijing Municipal Commission of Education (20111001002), and the Fundamental Research Funds for the Central Universities (ZY1325). M.W. particularly appreciates the financial aid from the China National Funds for Distinguished Young Scientists of the NSFC.

■ REFERENCES

(1) Reuther, J. F.; Novak, B. M. Evidence of entropy-driven bistability through ^{15}N NMR analysis of a temperature-and solvent-induced, chiroptical switching polycarbodiimide. *J. Am. Chem. Soc.* **2013**, *135*, 19292−19303.
(2) Lauceri, R.; Raudino, A.; Scolaro, L. M.; Micali, N.; Purrello, R. From achiral porphyrins to template-imprinted chiral aggregates and further self-replication of chiral memory from scratch. *J. Am. Chem. Soc.* **2002**, *124*, 894−895.
(3) Duan, P. F.; Qin, L.; Liu, M. H. Langmuir-blodgett films and chiroptical switch of an azobenzene-containing dendron regulated by the in situ host-guest reaction at the air/water interface. *Langmuir* **2011**, *27*, 1326−1331.
(4) Liu, L. B.; Hong, D. J.; Lee, M. Chiral assembly from achiral rod-coil molecules triggered by compression at the air-water interface. *Langmuir* **2009**, *25*, 5061−5067.
(5) Fendt, L. A.; Bouamaied, I.; Thöni, S.; Amiot, N.; Stulz, E. DNA as supramolecular scaffold for porphyrin arrays on the nanometer scale. *J. Am. Chem. Soc.* **2007**, *129*, 15319−15329.
(6) George, J.; Thomas, K. G. Surface plasmon coupled circular dichroism of Au nanoparticles on peptide nanotubes. *J. Am. Chem. Soc.* **2010**, *132*, 2502−2503.
(7) Shemer, G.; Krichevski, O.; Markovich, G.; Molotsky, T.; Lubitz, I.; Kotlyar, A. B. Chirality of silver nanoparticles synthesized on DNA. *J. Am. Chem. Soc.* **2006**, *128*, 11006−11007.
(8) Hiroshi, M.; Ayako, H.; Fumihiko, Y.; Takuya, M.; Tomoji, K. High-density DNA Alignment on an Au(111) Surface Starting from Folded DNA. *J. Am. Chem. Soc.* **2008**, *130*, 5002−5003.
(9) Lv, C. M.; Zou, D.; Qin, M.; Meng, W.; Cao, Y.; Wang, W. Hydrodynamic force depends not only on the viscosity of solution but also on the molecular weights of viscogens. *Langmuir* **2013**, *29*, 10624−10629.
(10) Schurr, J. M.; Smith, S. B. Theory for the extension of a linear polyelectrolyte attached at one end in an electric field. *Biopolymers* **1990**, *29*, 1161−1165.
(11) Dias, R.; Mel'nikov, S.; Lindman, B.; Miguel, M. G. DNA phase behavior in the presence of oppositely charged surfactants. *Langmuir* **2000**, *16*, 9577−9583.
(12) Stigter, D.; Bustamante, C. Theory for the hydrodynamic and electrophoretic stretch of tethered B-DNA. *Biophys. J.* **1998**, *75*, 1197−1210.

(13) Gurrieri, S.; Smith, S. B.; Bustamante, C. Trapping of megabase-sized DNA molecules during agarose gel electrophoresis. *Proc. Natl. Acad. Sci. U.S.A.* **1999**, *96*, 453−458.
(14) Norden, B.; Elvingsion, C.; Jonsson, M.; Akerman, A. Microscopic behaviour of DNA during electrophoresis: Electrophoretic orientation. *Q. Rev. Biophys.* **1991**, *24*, 103−164.
(15) Balducci, A. G.; Tang, J.; Doyle, P. S. Electrophoretic stretching of DNA molecules in cross-slot nanoslit channels. *Macromolecules* **2008**, *41*, 9914−9918.
(16) Gu, Q.; Cheng, C.; Gonela, R.; Suryanarayanan, S.; Anabathula, S.; Dai, K.; Haynie, D. T. Cobalt metallization of DNA: Toward magnetic nanowires. *Nanotechnology* **2005**, *16*, 1358−1363.
(17) Yu, G. H.; Kushwaha, A.; Lee, J. K.; Shaqfeh, E. S. G.; Bao, Z. The shear flow processing of controlled DNA tethering and stretching for organic molecule electronics. *ACS Nano* **2011**, *5*, 275−282.
(18) Adamcik, J.; Tobenas, S.; Santo, G. D.; Klinov, D.; Dietler, G. Temperature-controlled assembly of high ordered/disordered dodecylamine layers on HOPG: Consequences for DNA patterning. *Langmuir* **2009**, *25*, 3159−3162.
(19) Williams, G. R.; O'Hare, D. Towards understanding, control and application of layered double hydroxide chemistry. *J. Mater. Chem.* **2006**, *16*, 3065−3074.
(20) Fogg, A. M.; Williams, G. R.; Chester, R.; O'Hare, D. A novel family of layered double hydroxides-$[MAl_4(OH)_{12}](NO_3)_2{\cdot}xH_2O$ (M = Co, Ni, Cu, Zn). *J. Mater. Chem.* **2004**, *14*, 2369−2371.
(21) Kong, X. G.; Rao, X. Y.; Han, J. B.; Wei, M.; Duan, X. Layer-by-layer assembly of bi-protein/layered double hydroxide ultrathin film and its electrocatalytic behavior for catechol. *Biosens. Bioelectron.* **2010**, *26*, 549−554.
(22) Wang, Q.; O'Hare, D. Recent advance in the synthesis and application of layered double hydroxide (LDH) nanosheets. *Chem. Rev.* **2012**, *112*, 4124−4155.
(23) Bontchev, P. P.; Liu, S.; Krumhansl, J. L.; Voigt, J. Synthesis, characterization, and ion exchange properties of hydrotalcite $Mg_6Al_2(OH)_{16}(A)_x(A')_{2-x}{\cdot}4H_2O$ (A, A′ = Cl^-, Br^-, I^-, and NO_3^-, $2 \geq x \geq 0$) derivatives. *Chem. Mater.* **2003**, *15*, 3669−3675.
(24) Spitz, C.; Dähne, S. Proof of chirality of J-aggregates spontaneously and enantioselectively generated from achiral dyes. *J. Phys. Chem. B* **2000**, *104*, 8664−8669.
(25) Saeva, F. D.; Olin, G. R. On the extrinsic circular dichroism of J-aggregate species of achiral dyes. *J. Am. Chem. Soc.* **1977**, *99*, 4848−4850.
(26) Reynolds, R. C. In *Modern Powder Diffraction*; Bish, D. L., Post, J. E., Eds.; Mineralogical Society of America, Washington, DC, 1989.
(27) Lang, J.; Liu, M. Layer-by-layer assembly of DNA films and their interactions with dyes. *J. Phys. Chem. B* **1999**, *103*, 11393−11397.
(28) Jiang, S.; Liu, M. A chiral switch based on dye-intercalated layer-by-layer assembled DNA film. *Chem. Mater.* **2004**, *16*, 3985−3987.
(29) Paulo, P. M. R.; Costa, S. M. B. Interactions in noncovalent PAMAM/TMPyP systems studied by fluorescence spectroscopy. *J. Phys. Chem. B* **2005**, *109*, 13928−13940.
(30) Kelly, J. M.; Murphy, M. J.; McConnell, D. J.; OhUigin, C. A study of the interactions of some polypyridylruthenium(II) complexes with DNA using fluorescence spectroscopy, topoisomerisation and thermal denaturation. *Nucleic Acids Res.* **1985**, *13*, 6017−6034.
(31) Lyng, R.; Rodger, A.; Nordén, B. The CD of ligand-DNA systems. 1. Poly(dG-dC) B-DNA. *Biopolymers* **1991**, *31*, 1709−1720.
(32) Lyng, R.; Rodger, A.; Nordén, B. The CD of ligand-DNA systems. 2. Poly(dA-dT) B-DNA. *Biopolymers* **1992**, *32*, 1201−1214.
(33) Magdalena, E.; Bengt, N. Linear and circular dichroism of drug-nucleic acid complexes. *Methods Enzymol.* **2001**, *340*, 68−98.
(34) Strickland, J.; Marzilli, L. G.; Wilson, W. D. Binding of meso-tetrakis(N-Methylpyridiniumyl) porphyrin isomers to DNA: Quantitative comparison of the influence of charge distribution and copper(II) derivatization. *Biopolymers* **1990**, *29*, 1307−1323.
(35) Wirth, M.; Buchardt, O.; Koch, T.; Nielsen, P. E.; Bengt, N. Interactions between DNA and Mono-, Bis-, Tris-, Tetrakis-, and Hexakis(aminoacridines). A linear and circular dichroism, electric orientation relaxation, viscometry, and equilibrium study. *J. Am. Chem. Soc.* **1988**, *110*, 932−939.
(36) Jiang, S.; Chen, X.; Liu, M. The pH stimulated reversible loading and release of a cationic dye in a layer-by-layer assembled DNA/PAH film. *J. Colloid Interface Sci.* **2004**, *277*, 396−403.
(37) Yamamoto, S.; Watarai, H. Surface-enhanced Raman spectroscopy of dodecanethiol-bound silver nanoparticles at the liquid/liquid interface. *Langmuir* **2006**, *22*, 6562−6569.
(38) Procházka, M.; Štěpánek, J.; Turpin, P. Y.; Bok, J. Drastically different porphyrin adsorption and metalation processes in chemically prepared and laser-ablated SERS-active silver colloidal substrates. *J. Phys. Chem. B* **2002**, *106*, 1543−1549.
(39) Thomas, G. J.; Tsuboi, M. Local raman tensors of double-helical DNA in the crystal: A basis for determining DNA residue orientations. *Adv. Biophys. Chem.* **1993**, *3*, 1−70.
(40) Duguid, J. G.; Bloomfield, V. A.; Benevides, J. M.; Thomas, G. J. DNA melting investigated by differential scanning calorimetry and Raman spectroscopy. *Biophys. J.* **1996**, *71*, 3350−3360.
(41) Dostal, L.; Chen, C. Y.; Wang, A. H. J.; Welfle, H. Partial B-to-A DNA transition upon minor groove binding of protein Sac7d monitored by Raman spectroscopy. *Biochemistry* **2004**, *43*, 9600−9609.
(42) Muntean, C. M.; Dostal, L.; Misselwitz, R.; Welfle, H. DNA structure at low pH values, in the presence of Mn^{2+} ions: A Raman study. *J. Raman Spectrosc.* **2005**, *36*, 1047−1051.
(43) Deng, H.; Bloomfield, V. A.; Benevides, J. M.; Thomas, G. J. Dependence of the Raman signature of genomic B-DNA on nucleotide base sequence. *Biopolymers* **1999**, *50*, 656−656.